Journal of Geoscience and Environment Protection, 2026, 14(4), 281-299
https://www.scirp.org/journal/gep
ISSN Online: 2327-4344
ISSN Print: 2327-4336

Distribution of Apparent Resistivities and Lithological Profiles of Soils in Penka-Michel, West Cameroon

Annie Christelle Djoumete Kengne, Jean Victor Kenfack*, Maurice Kwekam, Malick Rosvelt Demanou Messe, Eric Donald Teikeu Ngueveu, Thierry Suffeu Talla, Marole Kouokam

Laboratory of Environmental Geology, Department of Earth Sciences, University of Dschang, Dschang, Cameroon
Email: *jvkenfi@yahoo.fr

How to cite this paper: Djoumete Kengne, A. C., Kenfack, J. V., Kwekam, M., Demanou Messe, M. R., Teikeu Ngueveu, E. D., Suffeu Talla, T., & Kouokam, M. (2026). Distribution of Apparent Resistivities and Lithological Profiles of Soils in Penka-Michel, West Cameroon. *Journal of Geoscience and Environment Protection, 14,* 281-299.
https://doi.org/10.4236/gep.2026.144015

Received: March 6, 2026
Accepted: April 25, 2026
Published: April 28, 2026

Abstract

This geophysical study conducted in the Penka-Michel region, in the West of Cameroon, analyzes the distribution of apparent resistivities and the lithological profiles of the soils, which are essential for road infrastructure planning. Vertical electrical soundings (VES) carried out at 51 points revealed a significant heterogeneity of resistivities at different depths (1.5 m to 27.5 m), corresponding to variations in the underlying materials. Areas with high resistivity, notably in the north and southwest, are dominated by more resistant materials, potentially exploitable for road construction. In contrast, areas with low resistivity, present in the east and south, indicate clayey or water-saturated soils, less suitable for road applications. These results provide the geophysical mapping needed to optimize the use of local resources and help improve the sustainability of infrastructure. Integrating geophysical data into soil management would help reduce costs, minimize the risk of premature degradation of infrastructures, and promote informed planning of road projects. This study fills an important gap in geophysical mapping in the region and calls for further research to refine the understanding of soils and their sustainable management in infrastructure projects.

Keywords

Apparent Resistivities, Lithological Profiles, Geotechnical Implications, Soils, Penka-Michel

1. Introduction

The planning, construction, and durability of linear infrastructures, particularly

roads, require a detailed understanding of the subsoil properties and the materials that compose it (Rasul et al., 2018). Indeed, the geophysical characteristics of soils, especially variations in electrical resistivity, are directly related to essential parameters for road construction such as texture, compaction, moisture content, and the state of geological horizons (Ademila et al., 2022). In tropical contexts with high pedological heterogeneity, the lack of accurate mapping of available materials, particularly aggregates and resistant horizons, poses a major obstacle to optimizing road pavement costs and durability, often leading to cost overruns, premature degradation, and risks of instability (Rasul et al., 2018).

The use of geophysical methods, particularly vertical electrical soundings (VES), allows the measurement of apparent resistivity of the subsoil, providing non-intrusive information about the structure of horizons and the distribution of materials at different depths (Telford et al., 1990). These measurements are fundamental because electrical resistivity varies significantly depending on the lithological nature of horizons, water saturation, porosity, and the content of coarse materials that may be used in road construction (Malick Rosvelt et al., 2022; Victor et al., 2025). In similar studies in Cameroon, the integration of geophysical data with geotechnical measurements has led to the proposal of urban soil maps identifying different classes of materials and resistivities, facilitating geotechnical decision-making prior to infrastructure work (Malick Rosvelt et al., 2022).

Detailed mapping of exploitable materials, as opposed to simple surface pedological or geological classifications, is still lacking in many areas of Central Africa, such as Penka Michel. The absence of such data on resistivities and lithological profiles limits the ability to identify areas with high potential for suitable materials for road foundation and base layers (Kearey et al., 2002). Methods such as electrical resistivity or electrical resistivity tomography (ERT) not only allow us to determine but also to visualize underlying structures, which is necessary for mapping layers suitable for reuse as backfill or subgrade materials in civil engineering.

In Cameroon, researchers such as Foko Tamba et al. (2022), Malick Rosvelt et al. (2022) have applied geoelectrical surveys to soil mapping in urban areas, showing that it is possible to correlate electrical properties with geotechnical classifications useful for engineering. These approaches align with the work of Victor et al. (2025), Rodrigue et al. (2022), who explored the relationships between resistivity and lithological types in metamorphic rock contexts, as well as contributions from Stephane et al. (2024) on the mapping of groundwater aquifers using geophysical methods.

Applied geophysics has a long tradition of use for understanding subsoil in heavy infrastructure projects. For instance, resistive methods have been used since the 1930 in road projects to identify granular material zones favorable for exploitation and to reduce the number of required boreholes (Ayodele et al., 2015). These techniques have been widely used to characterize soil properties and optimize material choices for construction, helping to identify areas suitable for the exploitation of aggregates, thus reducing drilling and excavation costs (Akintorinwa, 2018). More

recent studies show that these methods, particularly electrical resistivity tomography (ERT), are still used in infrastructure planning, providing a detailed view of subsoil structures and enabling informed decisions about construction materials (Alam et al., 2024). More recently, geophysical applications combined with geotechnical data have been used to develop integrated maps of available materials in a given area, which is essential for road planning, defining pavement thickness, and optimizing local resources (Ademila et al., 2022; Sangprasat et al., 2025).

In the specific context of Penka Michel, located in the West of Cameroon on a varied geological complex, no detailed mapping of potentially exploitable materials for road construction is currently available. The lack of such data leads to significant uncertainty in identifying areas suitable for foundation or base materials, which complicates technical and economic decisions during infrastructure design. This study aims to fill this gap by providing an analysis of apparent resistivities and lithological profiles through geoelectrical surveys, thus paving the way for geophysical mapping of subsoil materials useful for road engineering and other projects involving soil resource utilization.

2. Methodology

The geophysical study of the Penka Michel area was conducted using vertical electrical soundings (VES), a technique commonly used for soil characterization due to its simplicity and efficiency in areas with high geological heterogeneity. This method relies on measuring the apparent resistivity of the soils based on the spacing of current and reception electrodes. The Schlumberger configuration was used for this study because it allows for deeper penetration of electrical surveys while maintaining a reasonable resolution of the underlying geological layers.

For each measurement station, a low-intensity current was injected through two current electrodes (A and B), while the potential difference was measured between two reception electrodes (M and N). The apparent resistivity (ρ_a) is calculated according to Ohm's law generalized for a homogeneous medium:

$$\rho_a = k\frac{U_{MN}}{I_{AB}}$$

where U_{MN} is the potential difference measured between the receiving electrodes, I_{AB} is the injected current, and k is a geometric factor that depends on the electrode spacing. This factor is given by the following expression for the Schlumberger configuration:

$$k = \frac{2\pi}{\frac{1}{r_{AM}} - \frac{1}{r_{BM}} - \frac{1}{r_{AN}} + \frac{1}{r_{BN}}}$$

where r_{AM}, r_{BM}, r_{AN}, and r_{BN} represent the respective distances between the current and reception electrodes.

For this study, approximately 66 survey points were planned, spaced 200 meters

apart to provide the widest possible coverage of the study area (Figure 1). The choice of a 200-meter spacing was motivated by changes in surface soil texture from one point to another, on the one hand, and topographic heterogeneity, on the other. Due to difficulties in accessing certain points, only 51 points were ultimately surveyed. Particular emphasis was placed on sampling points requiring a complete geotechnical characterization. The measurements were performed at various distances between the current electrodes (*AB*), allowing the exploration of apparent resistivities at increasing depths, ranging from 1.5 m to 27.5 m. This approach provides information on resistivity variations at different depths, offering a detailed view of the subsoil characteristics. The geoelectric measurements are then georeferenced and integrated into a Geographic Information System. Spatial interpolation tools (kriging) are used to estimate the distribution of resistivities, taking into account the spatial structure of the data.

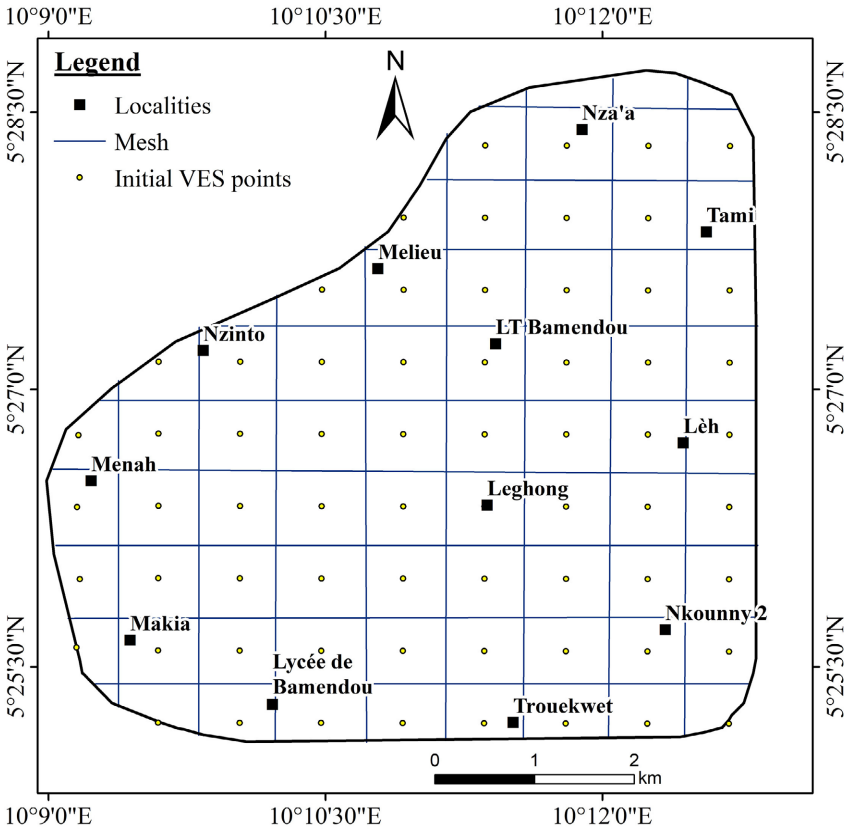

Figure 1. Spatial distribution of the proposed survey points.

Once the data was collected, it was processed and interpreted using the JOINTEM 1.4 software, a geophysical inversion tool commonly used for vertical electrical sounding data. JOINTEM is a software that performs 1D inversion of apparent resistivity data, allowing the estimation of the true resistivities of the underlying geological layers as well as their thickness. The software uses inversion methods based on a nonlinear optimization algorithm to minimize the difference between the measured resistivities and those calculated by a model with horizontal layers.

The goal is to find a resistivity distribution that best matches the observed data by adjusting the model parameters at each depth (Telford et al., 1990).

The inversion algorithm used by JOINTEM 1.4 is based on the least squares method to solve the inversion equation. The fundamental inversion equation is given by:

$$\sum_{i=1}^{N}\left(\rho_a^{meas}\left(x_i\right)-\rho_a^{calc}\left(x_i\right)\right)^2 \to \min$$

where $\rho_a^{meas}\left(x_i\right)$ is the apparent resistivity measured at position x_i, and $\rho_a^{calc}\left(x_i\right)$ is the apparent resistivity calculated from the inversion model. The method minimizes the sum of the squared differences between the measured resistivities and the calculated resistivities across all measurement stations. The inversion results provide the true resistivity of the different geological layers as well as their depth, allowing the generation of a complete geophysical profile of the subsoil.

The model used for the inversion assumes that the soils are composed of horizontal layers with uniform resistivity. The thickness of each layer is an adjustable parameter during the inversion process. The use of JOINTEM version 1.4 software allows for the simulation of different soil configurations and provides a reliable estimation of the resistivity distribution and underlying geological structures. To process data in the JOINTEM software for generating 1D inversion curves, the first step is to collect and convert the data into a DAT file. The 1D inversion was performed using a homogeneous initial model consisting of 3 - 5 layers, with an average RMS (Root Mean Square) error of 5%.

Lithological profiles are generated using Strater 5 software, which represents the succession of soil layers at each sounding point. From the lithological profiles, the thickness of the underlying soil layers and the investigation depth are also observed.

The resistivity data obtained were statistically analyzed to understand the spatial variability of resistivities and material properties with depth. Descriptive statistics include means, standard deviations, and spatial variability analysis. These analyses help create an apparent resistivity map for each depth, providing crucial information for material evaluation, particularly in terms of their suitability for use in road construction projects.

The particular problem of Penka-Michel lies in the absence of accurate mapping of exploitable materials for road construction. This shortcoming hinders the optimal management of local resources and complicates road infrastructure planning. In the absence of such geophysical maps, construction material choices are often based on point samples that are not representative, leading to additional costs and durability issues for roads constructed in this area.

3. Results and Discussion

The spatial distribution of the 51 bridges that were actually surveyed is shown in Figure 2. The interpretation of the VES curves allows for the identification of dif-

ferent geological layers, estimation of their thickness, and determination of the vertical distribution of lateritic horizons, which are essential information for the design of road foundations.

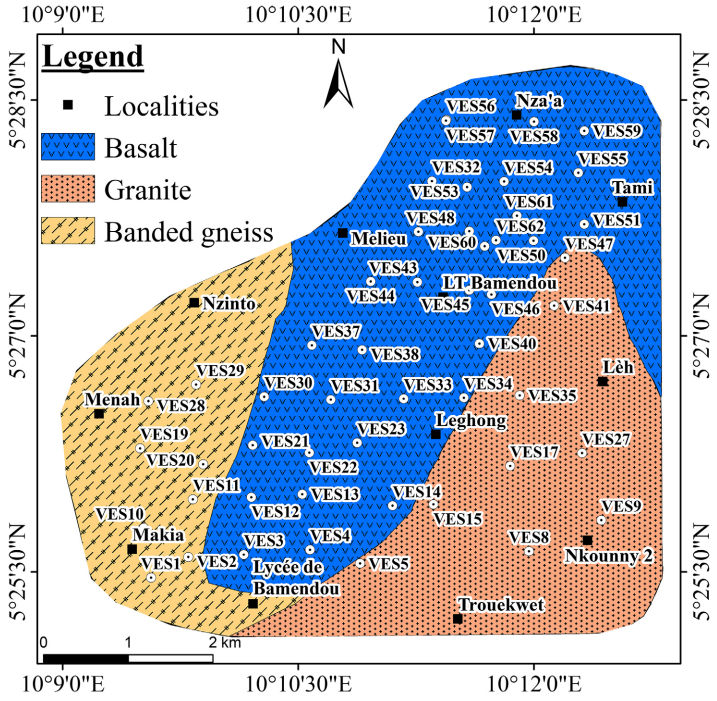

Figure 2. Spatial distribution map of VES.

3.1. Distribution of Apparent Resistivities

3.1.1. Analysis of Variations in Apparent Resistivity at Different Pseudo-Depths (1.5 m to 27.5 m)

The apparent resistivity measurements obtained through vertical electrical soundings (VES) show significant variations across different depths. At shallow depths (1.5 m), the observed values are generally low, which often corresponds to horizons rich in clay or high in water content, characteristics associated with high conductivity and low resistivity. This strong variability of resistivity at the surface is consistent with the observations of Montoroi et al. (1997), who note that local hydric conditions strongly control the resistivity of upper horizons: the higher the moisture, the lower the apparent resistivity, which is typical of humid tropical soils similar to those in Penka Michel.

At intermediate depths (6.3 m to 13.2 m), resistivities increase markedly, reflecting more resistant geological horizons, likely dominated by compacted sands or gravels. This behavior is also explained in the international literature, where the increase in resistivity with depth is interpreted as the effect of decreased water content and an increase in compaction and material heterogeneity. At greater depths (19 m to 27.5 m), some points show very high resistivities (>5000 Ω·m), indicating the presence of very compact rock formations or low-porosity materials, potentially exploitable as aggregates for road construction

(Hacini, 2006).

The vertical variation in resistivities observed follows the classical geophysical logic commonly documented for VES: deeper layers are generally more resistive due to lower water saturation and the predominance of more cohesive materials (Kearey & Brooks, 1991).

3.1.2. Iso-Resistivity Maps and Discussion on High and Low Resistivity Zones

The resistivity maps obtained show a heterogeneous geographical distribution of apparent resistivities at all pseudo-depth levels, reflecting the heterogeneity of the subsurface materials in the study area. For example, the northern and southwestern areas generally exhibit higher resistivity values, which is consistent with more compact geological layers, likely sandy or coarse-textured, which are known to exhibit high electrical resistivities. These areas could correspond to materials potentially usable for road construction.

In contrast, the southern and eastern areas show relatively low resistivities, sometimes below 500 Ω·m, indicating more clayey materials or water-saturated horizons, typical of less dense terrains that are less favorable for supporting road loads (Montoroi et al., 1997). In applied geophysics, resistivity mapping is often interpreted in conjunction with hydrogeological data: low resistivity is a reliable indicator of fine, saturated materials, while high resistivity suggests coarse or compacted materials, favorable for soil engineering.

These maps highlight areas that, from a geophysical perspective, show potential for exploitation for pavement materials, particularly in the northern and southwestern sectors, reinforcing the need for further analyses (controlled drilling, geotechnical tests) to validate this potential.

3.1.3. Comparison of Resistivities Across Different Pseudo-Depths and Geographic Regions (North, South, East, West)

The apparent resistivity values presented here were obtained at various depths from the previously mentioned points. These depths, considered as pseudo-depths (**Figure 3**), correspond to the following values: AB/2 = 1.5 m, AB/2 = 2.1 m, AB/2 = 3 m, AB/2 = 4.4 m, AB/2 = 6.3 m, AB/2 = 9.1 m, AB/2 = 13.2 m, AB/2 = 19 m, and AB/2 = 27.5 m.

From AB/2 = 1.5 m to AB/2 = 4.4 m (**Figure 3(a)**), the apparent resistivity values range from 138.05 Ω·m to 635.45 Ω·m. The highest values (363.97 Ω·m to 635.41 Ω·m) in this range are found in the North, South, and Southwest of the study area.

For AB/2 = 6.3 m (**Figure 3(b)**), the resistivity values range from 352.93 Ω·m to 935.99 Ω·m. Only the locality of Nza'a in the North presents the highest resistivity values at this depth, ranging from 573.02 Ω·m to 935.99 Ω·m. The areas with medium resistivities (491.29 Ω·m to 573.01 Ω·m) are located in the South and Southwest. The lowest resistivity values (352.93 Ω·m to 491.28 Ω·m) are found in the South-Southwest, Northwest, and East.

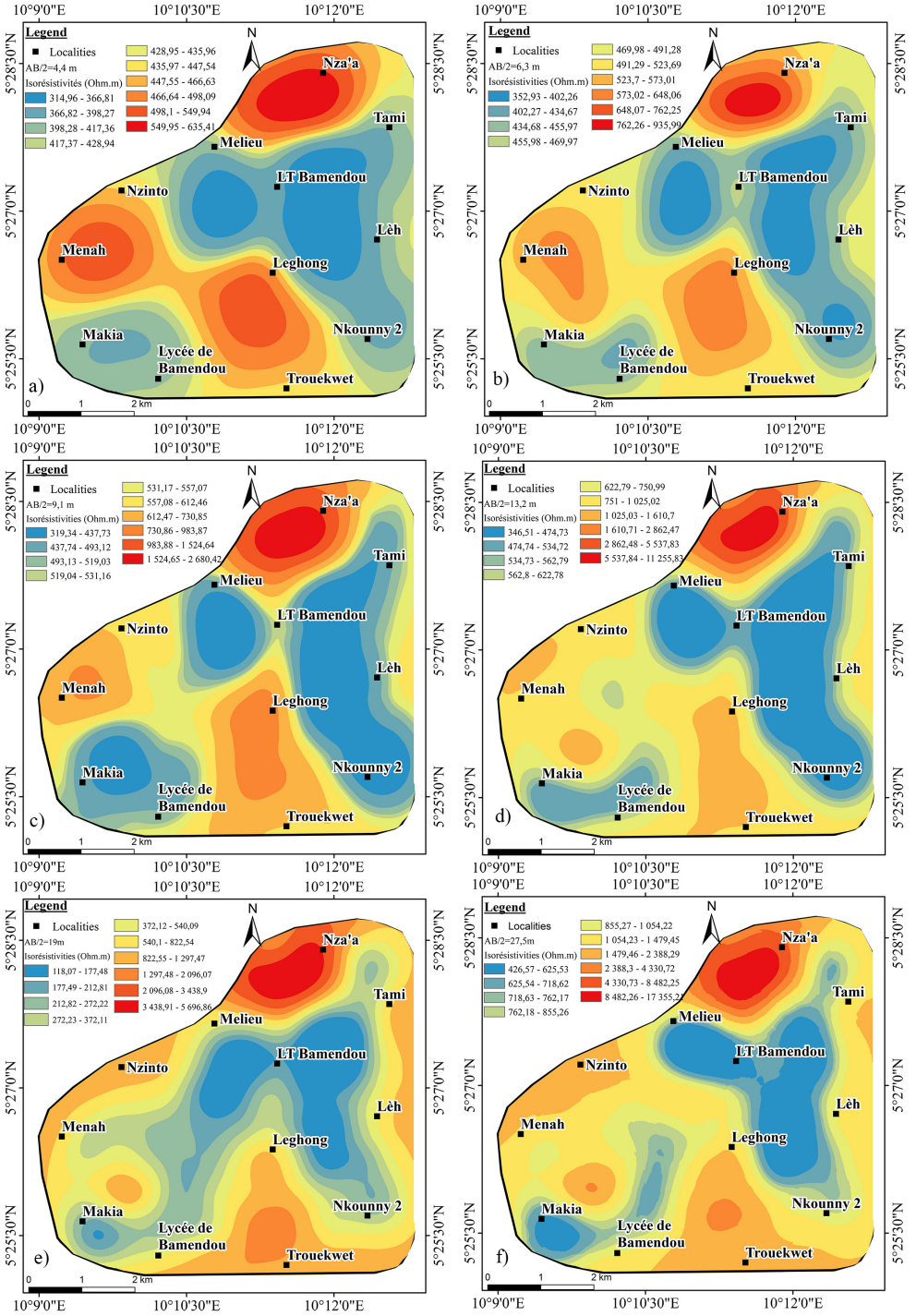

Figure 3. Apparent resistivity iso-maps.

For AB/2 = 9.1 m (**Figure 3(c)**), the resistivity values are low, ranging from 319.34 Ω·m to 2680.42 Ω·m. The North alone hosts the highest resistivities, ranging from 730.86 Ω·m to 2680.42 Ω·m; the medium resistivities are concentrated in the South and West, ranging from 537.17 Ω·m to 730.85 Ω·m; and the lowest values, ranging from 319.34 Ω·m to 537.16 Ω·m, are concentrated in the South-West, North-West, and East.

For AB/2 = 13.2 m (Figure 3(d)), the resistivity values range from 346.51 Ω·m to 11,255.83 Ω·m. The highest resistivity values, like in the previous range, are concentrated in the North, ranging from 1610.71 Ω·m to 11,255.83 Ω·m. The medium values (622.79 Ω·m to 1610.70 Ω·m) cover most of the area, including the South, East, and West. The lowest values (346.51 Ω·m to 622.78 Ω·m) are more concentrated in the Northwest, South-Southwest, Northeast, and Southeast.

For AB/2 = 19 m (Figure 3(e)), the resistivity values range from 402.10 Ω·m to 7139.68 Ω·m. The highest resistivities (1297.48 Ω·m to 5696.86 Ω·m) at this depth are found in the locality of Nza'a in the North, with a small pocket in the South. The South, West, and East borders are areas where medium resistivities (372.12 Ω·m to 822.54 Ω·m) are located. The lowest resistivities are found in the South-Southwest, Center, Northeast, and Southeast.

For AB/2 = 27.5 m (Figure 3(f)), the electrical resistivity values range from 426.57 Ω·m to 17,355.21 Ω·m. The locality of Nza'a remains the one presenting the highest resistivities at this depth, ranging from 2383.14 Ω·m to 17,284.18 Ω·m. The medium resistivities at this depth are found in the South, West, and East. The lowest resistivities are more concentrated in the South-Southwest, Center, and East, ranging from 426.57 Ω·m to 1054.22 Ω·m.

The spatial comparison of resistivities by depth reveals marked differences between the geographical sectors. At intermediate and deeper depths, the North and Southwest consistently present higher resistivities than the East and Southeast zones, suggesting lateral variation in lithological properties. Such lateral contrasts are well documented in several geophysical studies, where more consolidated or less hydrated formations result in higher resistivities compared to more conductive clayey or alluvial formations.

This lateral variation is significant from a soil engineering perspective: it indicates that the suitability of subsoil materials to support loads and be used as foundation or base materials is not homogeneous across the entire study area. The sectors with high resistivities may offer more resistant and less saturated materials, reducing the risks of deformation under load (Hacini, 2006).

3.2. Lithological Soil Profiles

3.2.1. Description of Lithological Profiles Obtained from Vertical Electrical Soundings (VES)

The lithological models derived from the VES data inversions reveal a stratified organization of subsurface materials (Figure 4). The upper horizon (<5 m) is generally dominated by fine materials (clays, silts), characterized by low to moderate resistivities, consistent with higher water content or less consolidated soils.

At greater depths, the profiles show layers with increasing resistivity, often associated with coarser sandy and gravelly formations that are less saturated, corresponding to the high resistivities measured in the soundings. Such vertical stratification aligns with classical models of tropical soils, where denser horizons may

develop beneath looser surface layers.

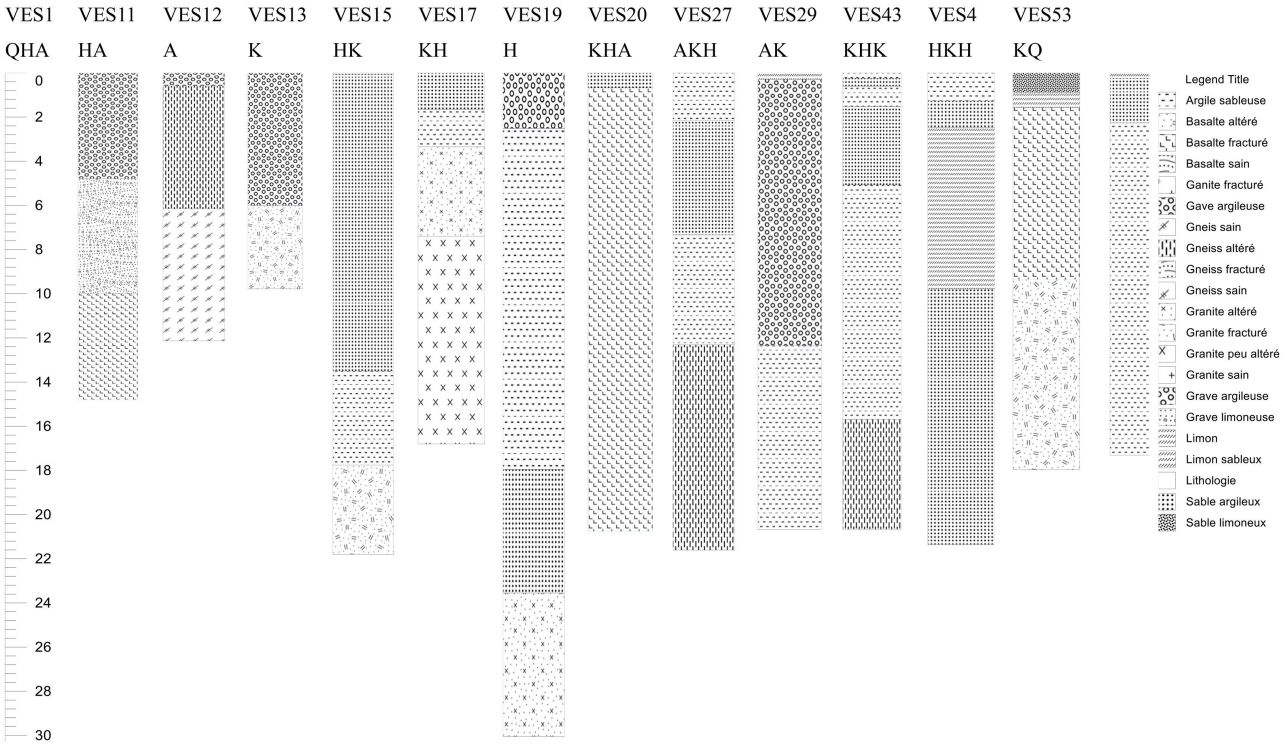

Figure 4. Lithological profiles at the locations of the representative sounding points.

3.2.2. Discussion on Identified Soil Types and Their Relationship with Apparent Resistivity

The relationship between the actual lithological nature of layers and the measured apparent resistivities is well documented: saturated clay soils exhibit low resistivities (<100 Ω·m), whereas sandy or gravelly formations show higher resistivities (>500 Ω·m). In the case of Penka Michel, this relationship is well corroborated: areas with low apparent resistivity are interpreted as clay-rich or highly hydrated horizons, which are unfavorable for the extraction of materials for road construction.

Conversely, areas with high resistivity, both laterally and vertically, indicate potentially more resistant and coherent horizons, associated with unsaturated sandy-gravelly materials, which are generally preferred for geotechnical engineering applications (Montoroi et al., 1997). These results should be interpreted with caution, as high resistivities may also result from specific hydro-mechanical conditions (low-ion water or low saturation), yet they nevertheless provide a robust basis for identifying zones with potential.

3.3. Geophysical Inversions and Curve Types

3.3.1. Analysis of Obtained 1D Inversion Curves

The 1D inversions performed (using JOINTEM) allowed the adjustment of subsurface resistivity models based on the measured apparent resistivities, producing profiles that typically distinguish several superimposed layers. These inversion

curves exhibit varied signatures, including bell-shaped models (KH) or more complex profiles (KHA, HKH) depending on the nature of the traversed layers: for example, a sharp change in resistivity may reflect the transition from a clay horizon to a compacted sandy horizon. Inversion curves are an essential tool in applied geophysics for modeling vertical resistivity variations and are discussed in detail in the classical literature on electrical methods (Telford et al., 1990).

3.3.2. Identification of Dominant Curve Types and Their Geophysical Significance

Thirteen types of VES curves were obtained following the processing of data from a total of 51 sounding points. The representative sounding points for all types of 1D inversion curves are shown in **Figure 5**. The interpretation of the patterns of the various types of curves is based on field observations, on the one hand, and on the literature, on the other hand. The dominant curve types observed in this study (KH, KHA) suggest two main configurations: gradual transitions from conductive to resistive materials, and intermediate layers with moderate resistivity. This behavior can be interpreted as the presence of sequences of contrasting geological layers, typical of areas with significant sediment heterogeneity. Such signatures have been previously discussed in similar contexts, where vertical resistivity variations are linked to alternations between loose superficial sedimentary sequences and more coherent deeper formations.

Type A curve (**Figure 5(a)**), or "stepped upward," indicates an increase in resistivity with depth. Two occurrences are identified in the northern sector of the western area of the Penka-Michel district, with resistivity values ranging from 99.99 Ω·m to 1101.74 Ω·m. These anomalies indicate a decrease in soil conductivity with depth. These are three-layer soils, of which the 99.99 Ω·m layer could consist of silty clays, the 188.02 Ω·m to 450.05 Ω·m layers would be sandy clays, and the 1101.74 Ω·m layer, of clayey sands, based on field observations and the results obtained after data processing (Palacky, 1991). Type AK curve (**Figure 5(b)**) combines anomalies of types A and K. Three occurrences were found in the study area: one in the west (VES29), another in the center (VES38), and one in the north (VES51), in the localities of Menah, Nzinto, and Tami, corresponding to VES12, VES54, and VES60. Resistivity values range from 254.5 Ω·m to 1544.32 Ω·m. Resistivity increases with depth up to approximately 16 m. Based on field observations and the resistivity ranges defined by Hoareau (2009), resistivities <400 correspond to weathered rocks, specifically clayey-silty sands. Type AKH curve (**Figure 5(c)**) combines A, K, and H features. Four occurrences were identified in the study area, located in Makia, Trouekwet, and Leh, in the southwest (VES2), south (VES4), and east (VES27 and VES35), respectively. The resistivities show a sawtooth pattern with depth, ranging from 76.51 Ω·m to 1934.51 Ω·m. These values may indicate the presence of clay and sandy-clay soils near the surface (<5 m) and weathered rock at greater depths.

Type H curve (**Figure 5(d)**), or "boat-shaped," reflects a considerable variation (decrease followed by increase) in resistivity with depth, with an almost constant

start from the surface to several meters deep. Two instances were recorded in the study area: one in the west (VES19) and one in the north (VES32), at Menah and Melieu, respectively. They indicate the presence of a moderately resistive layer between two more resistive layers. The resistivities here range from 578.37 Ω·m to 7515.7 Ω·m. The layers with resistivities ranging from 578.37 Ω·m to 586.7 Ω·m may correspond to sandy clays, those ranging from 916.67 Ω·m to 1118.35 Ω·m are similar to clayey sands, and those ranging from 2294.19 Ω·m to 7515.7 Ω·m to clayey gravels (Marescot, 2006). Type HA curve (**Figure 5(e)**) combines H and A anomalies. Unique in the study area, it is found in Makia, southwest (VES11). Type HK curve (**Figure 5(f)**) combines the "boat bottom" and "bell" shapes. Three curves of this type were obtained: one in the south (VES15) and two in the north (VES56 and VES57), at Leghong and Nza'a. This configuration shows an increase in resistivity with depth, but with the second soil layer being less resistive. Unique to the study area, it is found in the town of Makia, in the southwest (VES11). Based on field observations and the Marescot (2006) chart, the surface layer resembles clayey sand followed by a layer of sandy clay resting on fractured rock.

Type HKH curve (**Figure 5(g)**) is a "bell" curve flanked by two "boat-shaped" curves. Two occurrences were recorded: one in the southeast (VES9) and one in the northwest (VES49), at Melieu and Nkounny2. This anomaly indicates a significant fluctuation in resistivity values and the presence of multiple soil layers with different characteristics at the point in question. At the surface, there may be a layer of clay resting on silt, followed by rock that is more or less weathered. Type K curve (**Figure 5(h)**), or "bell-shaped," has two instances: one in the south (VES13) and one in the north (VES58), at Leghong and Nza'a. This is a representation of a three-layer soil profile in which the second layer is more resistive than the other two. The resistivity values range from 310.61 Ω·m to 15,031 Ω·m. The layers with resistivities between 310.61 Ω·m and 444.24 Ω·m could correspond to sandy clays, those between 1160.8 Ω·m and 5355.43 Ω·m to clayey sands, and the layer at 15,031 Ω·m to weathered gneiss (Palacky, 1991; Teikeu Ngueveu et al., 2025). Type KH curve (**Figure 5(i)**), combining K and H curves, features two contrasting domains—one "bell" followed by one "boat"—and is the most dominant and widespread in the study area, with a total of 19/51 occurrences (VES3, VES8, VES10, VES17, VES21, VES22, VES23, VES28, VES30, VES31, VES33, VES34, VES41, VES45, VES46, VES47, VES48, VES55, and VES59). It is concentrated mainly in the center but is also present in the north, south, west, and east. It is more concentrated in the center and, in a sense, reflects the general configuration of the subsurface in the study area. A statistical analysis revealed that this type of anomaly in the study area exhibits resistivities ranging from 49.11 Ω·m for the most conductive layers to 321,892.56 Ω·m for the least conductive layers. The VES3 at which this low resistivity value was obtained at a depth of 10.64 m indicates the presence of weathered granite (Tesis, 2010), 7.83 m thick; since at the same point and at a depth of 8.84 m, a resistivity value of 9306.56 Ω·m was recorded, corresponding to clayey gravel (Marescot, 2006). The maximum resistivity value of 321,892.56 Ω·m recorded at VES10 at a depth of 2.89 m indicates the presence of basalt (Palacky, 1991).

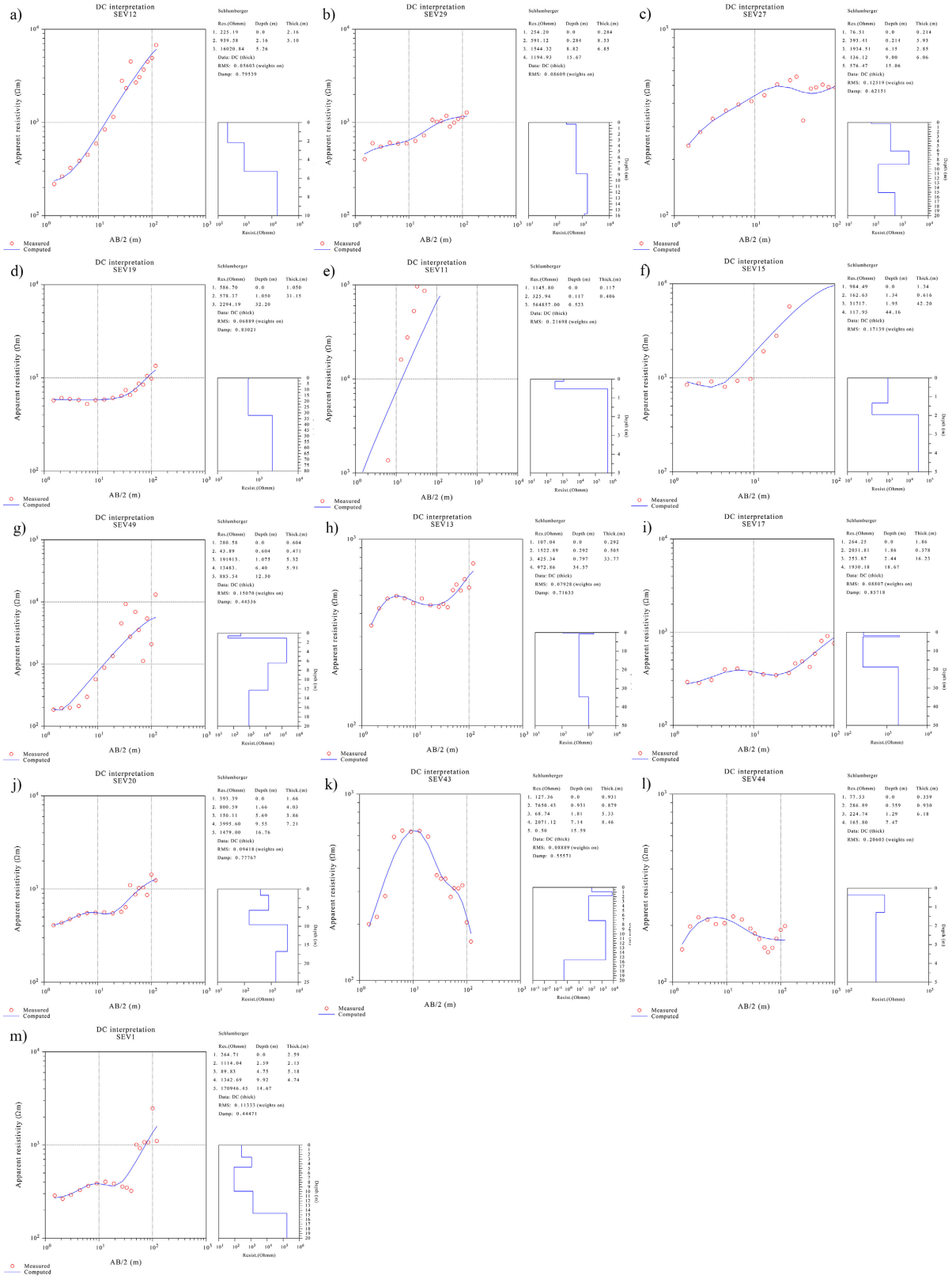

Figure 5. Typology of 1D inversion curves in the study area. (a) Type A curve; (b) Type AK curve; (c) Type AKH curve; (d) Type H curve; (e) Type HA curve; (f) Type HK curve; (g) Type HKH curve; (h) Type K curve; (i) Type KH curve; (j) Type KHA curve; (k) Type KHK curve; (l) Type KQ curve; (m) Type QHA curve.

Type KHA curve (**Figure 5(j)**) has the same combination as KH but with a different arrangement due to the sequence of curves; it is the most frequent in the study area, totaling 5/31. They rank second in the study area (5/13). This reflects an alternation between resistive and conductive layers at the points in question. The resistivity values of these types of anomalies in the study area range from 31.4 Ω·m to 188,302.70 Ω·m. This low resistivity value measured at VES61 at a depth of 0.152 m indicates the presence of silty clays (Palacky, 1991). Type KHK curve (**Figure 5(k)**) is the inverse of KHA, with two occurrences: one in the northwest (VES43) and one in the northeast (VES50), at Melieu and Tami. This anomaly indicates variations in resistivity values and the presence of multiple soil layers with different characteristics at the point in question. Analysis of the resistivity values reveals the presence of clay and sandy-clay soils near the surface and weathered rock at depth. Type KQ curve (**Figure 5(l)**) was identified once in the north (VES53, Nza'a) and twice in the west. Its combined shape reflects a resistivity increase from the surface to 1.55 m depth, followed by a decrease from 1.55 m to 11.82 m, after which a significant resistivity increase occurs. The resistivity values here may indicate the presence of loamy-clay soils at the surface, followed by clayey gravel at depth, all resting on more or less weathered bedrock.

Type QHA curve (**Figure 5(m)**) combines Q, H, and A curves and is characterized by three variation levels: a "boat bottom" between descending and ascending branches. The descending branch and boat bottom reflect a resistivity decrease from the surface to 9.92 m depth, while the ascending branch shows an increase from 9.92 m to 14.67 m. It is the only curve of this type in the study area, located in the southwest (VES1) in Makia. Analysis of the resistivity values indicates the presence of a surface clay layer, resting on clayey-lateritic gravel down to a depth of approximately 9 meters, and then on fractured rock that appears to be filled with compact clay.

3.4. Statistical Analysis of the Data

3.4.1. Calculation of Means, Standard Deviations, and Analysis of Resistivity Variability in the Study Area

The statistical analysis of apparent resistivities measured at the stations in Table 1 shows a significant dispersion of values both in amplitude and depth. This variability is reflected in high means and standard deviations, illustrating pronounced heterogeneity in the subsurface properties across the study area.

Among the analyzed data, some resistivities reach very high values (e.g., up to approximately 170,946 Ω·m at station VES1), while others exhibit much lower values (<100 Ω·m at VES27 or VES53). This wide range reflects strong lithological contrasts, associated with variations in texture, water saturation, and porosity of subsurface materials (as electrical resistivity depends on these parameters).

High electrical resistivity values are generally associated with dry, resistant, or poorly saturated materials (fractured rocks, sandstone, coarse materials), whereas low values indicate conductive materials, typically clay-rich or water-

saturated (colluvial soils, deep clays); this relationship between resistivity and soil saturation/texture is well documented in geophysical literature (Stephane et al., 2024).

In geotechnical studies, electrical resistivity is strongly influenced by soil moisture content and clay fraction: increased water content generally reduces resistivity through enhanced ionic conduction in pores, as reported by several authors (Sadegh et al., 2018). Conversely, dry soils or deep rock horizons exhibit high resistivity.

The statistical variability observed in this study, characterized by high means accompanied by large standard deviations, confirms that the subsurface is spatially heterogeneous, with materials that cannot be considered homogeneous at the regional scale. This resistivity heterogeneity aligns with the findings of Montoroi et al. (1997) and other similar studies, which show that lateral and vertical resistivity variations reflect lithological and hydric contrasts, depending on horizon thickness, texture, and soil water content (Montoroi et al., 1997).

3.4.2. Statistical Interpretation and Geophysical Implications

The statistical variations observed in **Table 1** confirm that the recorded resistivities are not uniform across the study area. This non-uniformity has significant implications for the geological and geotechnical interpretation of the data.

On one hand, the strong spatial variability of resistivities indicates that subsurface materials vary considerably in terms of composition, texture, and water saturation. This observation is consistent with geophysical knowledge, which attributes electrical resistivity primarily to soil moisture content and porosity, followed by mineralogy and texture (Stephane et al., 2024). For example, in tropical or colluvial soils, resistivity differences may reflect transitions between saturated clay horizons and drier granular horizons, as illustrated by the highly contrasting resistivity profiles in this study.

On the other hand, this variability shows that a uniform approach to geotechnical interpretation (such as considering the subsurface as homogeneous) would be scientifically inappropriate. Measured resistivities must be interpreted locally according to the geological context of each station, as increases or decreases in resistivity may indicate either lithological variations (e.g., transition from a sandy horizon to a clayey horizon) or hydric contrasts (more saturated versus drier zones) (Kearey et al., 2002; Stephane et al., 2024).

The observed electrical resistivity heterogeneity thus reinforces the need to integrate a multi-parameter geophysical approach to characterize subsurface materials prior to any infrastructure planning or design. Indeed, when combined with other geotechnical methods, electrical resistivity can enhance the structural resolution of subsurface models and improve the identification of potentially problematic zones (saturated areas, low-bearing-capacity horizons, conductive clay layers) (Stephane et al., 2024; Kearey et al., 2002).

Table 1. Summary of the various VES points.

Station	Nombre de Couches	N°	ρ (Ω·m)	Depth1	Depth2	Types
VES1	5	1	264.71	0	2.59	QHA
		2	1114.04	2.59	4.75	
		3	89.83	4.75	9.92	
		4	1342.69	9.92	14.67	
		5	170946.45	14.67		
VES11	4	1	2374.2	0	0.126	HA
		2	182.51	0.126	0.726	
		3	3717	0.726	10.73	
		4	3717.03	10.73		
VES 12	3	1	225.19	0	2.16	A
		2	939.58	2.16	5.26	
		3	16020.84	5.26		
VES13	3	1	444.24	0	44.01	K
		2	2278.24	44.01	44.2	
		3	1160.8	44.2		
VES15	4	1	884.49	0	1.34	HK
		2	162.63	1.34	1.95	
		3	31717	1.95	44.16	
		4	117.95	44.16		
VES17	4	1	264.25	0	1.86	KH
		2	2051.81	1.86	2.44	
		3	253.87	2.44	18.67	
		4	1930.18	18.67		
VES 19	3	1	586.7	0	1.05	H
		2	578.37	1.05	32.2	
		3	2294.19	32.2		
VES20	5	1	393.39	0	1.66	KHA
		2	800.59	1.66	5.69	
		3	150.11	5.69	9.55	
		4	3995.6	9.55	16.76	
		5	1479	16.76		
VES27	5	1	76.51	0	0.214	AKH
		2	393.41	0.214	6.15	
		3	1934.51	6.15	9	
		4	136.12	9	15.06	
		5	576.47	15.06		
VES29	4	1	254.2	0	0.284	AK
		2	291.12	0.284	8.82	
		3	1544.32	8.82	15.67	
		4	1194.93	15.67		

Continued

VES43	5	1	127.36	0	0.931	KHK
		2	7650.43	0.931	1.81	
		3	68.74	1.81	7.14	
		4	2071.12	7.14	15.59	
		5	0.5	15.59		
VES49	5	1	280.58	0	0.604	HKH
		2	43.89	0.604	1.075	
		3	191913	1.075	6.4	
		4	13483	6.4	12.3	
		5	885.54	12.3		
VES53	4	1	31.99	0	0.165	KQ
		2	16575	0.165	1.55	
		3	264.93	1.55	11.82	
		4	22235.72	11.82		

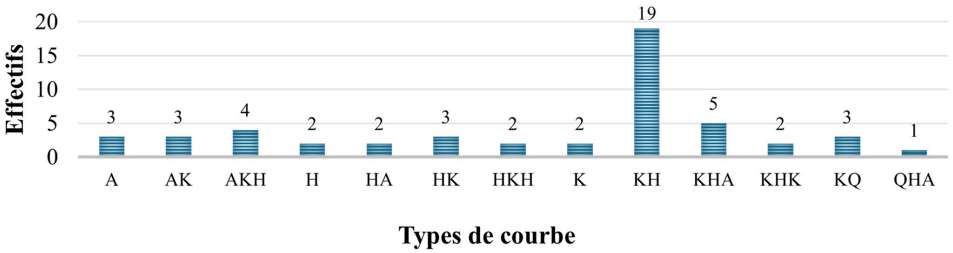

Figure 6. Histogram of the frequencies of the 13 types of 1D inversion curves in the study area.

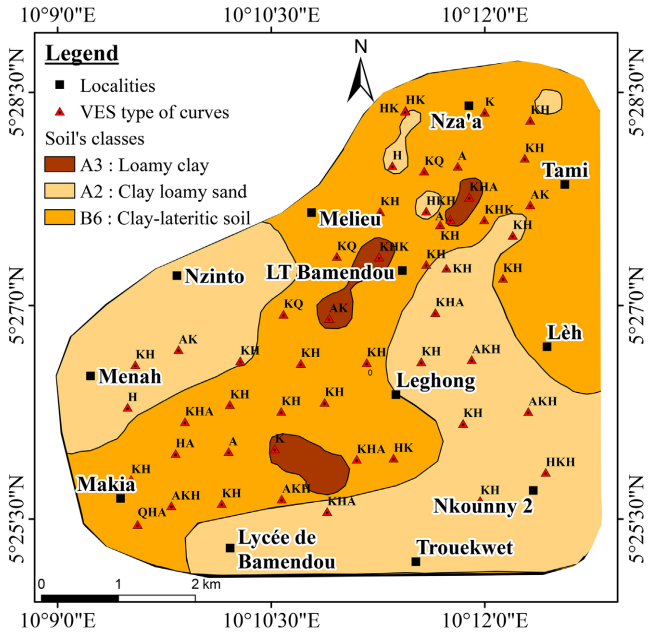

Figure 7. Spatial distribution of the different curve types at each VES point in the study area.

The number and frequency of the different curve types (**Figure 6**) provide information on the heterogeneous nature of the soil structure in the study area and the high variability of their sensitivity to electrical current flow. This sensitivity, in turn, is related either to the soil's grain-size distribution or to its moisture content at the time of the survey (Sadegh et al., 2018). **Figure 7** shows the spatial distribution of the curves, overlaid on the surface soils.

4. Conclusion

The geophysical study conducted at Penka-Michel, in western Cameroon, enabled a detailed characterization of the distribution of apparent resistivities and the lithological soil profiles, providing essential data for road infrastructure planning. The results show significant resistivity variability across the study area, with some sectors containing resistant materials suitable for road foundations, and others, more clayey or saturated, being less appropriate for construction.

These findings provide a solid basis for managing local resources, optimizing material selection, and reducing costs associated with road construction. Integrating geophysical data into geotechnical planning and soil management can help prevent premature infrastructure degradation and support informed decision-making. However, to refine this analysis and complete soil mapping, further studies combining geophysical data with geotechnical investigations would be necessary. Such an approach could greatly enhance the durability and efficiency of road infrastructure projects in the region.

Conflicts of Interest

The authors declare no conflicts of interest regarding the publication of this paper.

References

Ademila, O. (2022). Pre-Foundation Geophysical Investigation of a Site for Structural Development in Oka, Nigeria. *NRIAG Journal of Astronomy and Geophysics, 11,* 81-112. https://doi.org/10.1080/20909977.2021.1953297

Akintorinwa, O. J. (2018). Empirical Relationships between Electrical Resistivity and Geotechnical Parameters. *Soil Dynamics and Earthquake Engineering, 104,* 22.

Alam, M. J. B., Ahmed, A., & Alam, M. Z. (2024). Application of Electrical Resistivity Tomography in Geotechnical and Geoenvironmental Engineering Aspect. *Geotechnics, 4,* 399-414. https://doi.org/10.3390/geotechnics4020022

Ayodele, Y. G., Akinlabi, E. T., & Ojo, B. (2015). An Engineering Site Characterization Using Geophysical Methods. *GEO International Journal, 5,* 4-8.

Foko Tamba, C., Kengni, L., Tematio, P., Manefouet, B. I., & Kenfack, J. V. (2022). Assessment of Lateritic Gravelled Materials for Use in Road Pavements in Cameroon. *Geotechnical and Geological Engineering, 40,* 4195-4215. https://doi.org/10.1007/s10706-022-02151-4

Hacini, Y. (2006). *Application des méthodes géophysiques à l'étude de deux sites (Kappelen et Grenchen) de l'aquifère poreux complexe du Seeland* (225 p.). Thèse de doctorat, Université de Lausane, faculté des géosciences et de l'environnement.

Hoareau, J. (2009). *Use of a Coupled Hydrogeophysical Approach for the Study of Aqui-*

fers—Applications to the Contexts of Basement and Sandy Coast (p. 167). Doctoral Thesis, Joseph Fourier University.

Kearey, P., & Brooks, M. (1991). *An Introduction to Geophysical Exploration* (2nd ed.). Blackwell Scientific Publications.

Kearey, P., Brooks, M., & Hill, I. (2002). *An Introduction to Geophysical Exploration* (Vol. 4). John Wiley & Sons.

Malick Rosvelt, D. M., Jean Victor, K., Isaac yannick, B., François, N., & Armand Sylvain Ludovic, W. (2022). Geotechnical Soil Mapping from Electrical and Mechanical Properties: Case Study of the Bafoussam Urban Area, West Cameroon. *Applied Computing and Geosciences, 13,* Article ID: 100078. https://doi.org/10.1016/j.acags.2021.100078

Marescot, L. (2006). Introduction à l'imagerie électrique du sous-sol. *Bulletins Des Séances De La Société Vaudoise Des Sciences Naturelles, 90,* 23-40.

Montoroi, J. P. (1997). Conductivité électrique de la solution du sol et d'extraits aqueux de sol. *Etude et Gestion des sols, 4,* 279-298.

Palacky, G. J. (1991). Airborne Resistivity Mapping. In G. J. Palacky (Ed.), *Geological Survey of Canada Paper* (pp. 86-22, 9-18). Geological Survey of Canada.

Rasul, A., Balzter, H., Ibrahim, G. R. F., Hameed, H. M., Wheeler, J., Adamu, B. et al. (2018). Applying Built-Up and Bare-Soil Indices from Landsat 8 to Cities in Dry Climates. *Land, 7,* Article No. 81. https://doi.org/10.3390/land7030081

Rodrigue, T. T., Victor, K. J., Lucas, K., Adoua, N. K., Le-sage, K. M., & Stéphane, T. T. (2022). Contribution of Vertical Electrical Soundings, Landsat 8 and SRTM Images to the Comparative Study of the Hydrogeological Characteristics of the Foto, Keleng and Foreké Areas, West Cameroon. *Heliyon, 8,* e09675. https://doi.org/10.1016/j.heliyon.2022.e09675

Sadegh, R., Issa, S., & Hamed, R. (2018). Corrélation empirique entre les paramètres géotechniques et géophysiques dans une zone de glissement de terrain (étude de cas: Glissement de terrain de nargeschal). *Journal of Earth Science Research, 22,* 195-204.

Sangprasat, K., Puttiwongrak, A., & Inazumi, S. (2025). Review of Correlations between Soil Electrical Resistivity and Geotechnical Properties. *Geosciences, 15,* Article No. 166. https://doi.org/10.3390/geosciences15050166

Stephane, T. T., Victor, K. J., Théophile, N., Donald, T. N. E., & Rodrigue, T. T. (2024). Contribution of Vertical Electric Sounding, Landsat 8 and SRTM Images to Hydrogeological Characterization: Case Study of Batié, West-Cameroon. *Arabian Journal of Geosciences, 17,* Article No. 173. https://doi.org/10.1007/s12517-024-11967-8

Teikeu Ngueveu, E. D., Kenfack, J. V., Njanko, T., Suffeu Talla, T. B., Nouwa Ngouateu, B. V. F., & Tchomtchoua Tagne, S. (2025). Influence of Physical Properties on the Mechanical Behavior of Foundation Soils: Case of Soils from Fokoué-Centre. *Journal of Geoscience and Environment Protection, 13,* 69-86. https://doi.org/10.4236/gep.2025.137004

Telford, W. M., Geldart, L. P., & Sheriff, R. E. (1990). *Applied Geophysics* (2nd ed.). Cambridge University Press. https://doi.org/10.1017/cbo9781139167932

Tesis (2010). *Implementacion del codigo zoneRes 2D para la modelacion directae inversa de datos de tomografía de resistividad électrica 2D*. Universidad Nacional Autonomade Mexico Ciudad Universitaria, 23-40, 90-91.

Victor, K. J., Rodrigue, T. T., Yannick, B. I., Malick Rosvelt, D. M., Stéphane, T. T., Annie Christelle, D. K. et al. (2025). Assessment of the Hydrogeological Potential of the North-Eastern Sector of the Town of Dschang (West Cameroon) Using Integrated Remote Sensing, Geophysics and Multi-Criteria Analysis. *The Egyptian Journal of Remote Sensing and Space Sciences, 28,* 484-511. https://doi.org/10.1016/j.ejrs.2025.07.003